FHIT low /pHER2 high signature in non-small cell lung cancer is predictive of anti-HER2 molecule efficacy

Jordan da Silva, Amina Jouida, Julien Ancel, Véronique Dalstein, Julie Routhier, Gonzague Delepine, Jérôme Cutrona, Antoine Jonquet, Maxime Dewolf, Philippe L. Birembaut, et al.

FHIT^{low}/pHER2^{high} signature in non-small cell lung cancer is predictive of anti-HER2 molecule efficacy

Jordan Da Silva,[1§] Amina Jouida,[1§] Julien Ancel,[1,2] Véronique Dalstein,[1,3] Julie Routhier,[1] Gonzague Delepine,[1,4] Jérôme Cutrona,[1] Antoine Jonquet,[1] Maxime Dewolf,[2] Philippe Birembaut,[1,3] Gaëtan Deslée,[1,2] Myriam Polette,[1,3] Béatrice Nawrocki-Raby[1,*]

[1]INSERM, Université de Reims Champagne Ardenne, P3Cell UMR-S 1250, SFR CAP SANTE, 51097 Reims, France

[2]CHU de Reims, Hôpital Maison Blanche, Service de pneumologie, 51092 Reims, France

[3]CHU de Reims, Hôpital Maison Blanche, Laboratoire de pathologie, 51092 Reims, France

[4]CHU de Reims, Hôpital Robert Debré, Service de chirurgie cardio-vasculaire et thoracique, 51092 Reims, France

[§]These authors contributed equally to this work

*Corresponding author

Running title: A new NSCLC subclass eligible for HER2 therapy

Address for correspondence: Béatrice Nawrocki-Raby, INSERM UMR-S 1250, CHU Maison Blanche, 45 rue Cognacq-Jay, F-51100 REIMS, France. Phone: +33.3.26.78.77.70; Fax: +33.3.26.06.58.61; e-mail: beatrice.raby@univ-reims.fr

Conflicts of interest: AmJ, MP and BNR are the inventors of the patent application PCT/EP2017/073874 filed on September 21, 2017 and claiming the priority of the patent application EP16306213.6 filed on September 22, 2016. The remaining authors declare no potential conflicts of interest.

Word count: 3990

Abstract

Despite its efficacy in solid tumours, in particular HER2+ breast cancer, HER2-targeted therapy has given rise to disappointing results in non-small cell lung cancer (NSCLC).

With the aim of refining the target population for anti-HER2 therapies in NSCLC, we investigated the relationships between HER2 and the tumour suppressor fragile histidine triad (FHIT) in lung tumour cells.

First, we observed a negative correlation between FHIT expression and the activated form of HER2 (pHER2) in NSCLC samples and in lung tumour cell lines. Moreover, the silencing or overexpression of FHIT in lung cell lines led to an increase or decrease of HER2 activity, respectively. We also demonstrated that two anti-HER2 drugs, irbinitinib and trastuzumab, restore a more epithelial phenotype and counteract cell invasiveness and growth of FHIT-silenced tumour cell lines. Finally, we showed that the $FHIT^{low}$/$pHER2^{high}$ phenotype predicts sensitivity to an anti-HER2 therapy in primary tumour cells from NSCLC patients.

Our results show that FHIT regulates the activity of HER2 in lung tumour cells and that FHIT-inactivated tumour cells are sensitive to HER2 inhibitors. A new subclass of patients with NSCLC may be eligible for an anti-HER2 therapy.

Keywords: NSCLC; FHIT; HER2; targeted therapy; tumour cell phenotype; EMT

Introduction

Lung cancer is the leading cause of cancer-related death worldwide. Non-small cell lung cancer (NSCLC) accounts for approximately 85% of lung cancers (1). During the last decades, the treatment strategies for malignant tumours, in particular NSCLC, have been dramatically changed. Molecular targeted therapy against driver genes has improved patients' outcomes as compared with conventional chemotherapies (2). However, a substantial proportion of NSCLC patients, in whom no molecular marker is found, is still not eligible for personalized medicine.

The human epidermal growth factor receptor 2 (HER2) is overexpressed/amplified in many cancers, especially in breast cancer, and treatment of HER2+ breast cancer patients with the anti-HER2 monoclonal antibody trastuzumab has revolutionized their outcome (3). Several other HER2-targeted therapies were thereafter developed. (4). As for breast cancer, other solid tumours as gastric, colon or biliary cancer benefit from HER2 therapies, highlighting potential transposability and applicability in various tumours (5). Regarding NSCLC, the role of HER2-targeting drugs as monotherapy or in combination with chemotherapy remains unclear. HER2 overexpression, principally evaluated by immunochemistry (IHC), was described as an unfavourable prognostic factor (6-8). Such observation provided a rationale for studying HER2-targeted therapies in NSCLC and various phase II trials were therefore performed. In these trials, trastuzumab was combined with conventional cytotoxic drugs (cisplastin and gemcitabine) or conjugated to emtansine. (6, 9, 10). All trials were negative on primary endpoints. However, some subsets of patients with a strong overexpression of HER2 had a relatively high response rate. It was concluded that additional investigations into HER2 pathway alterations are necessary to clarify the efficacy of HER2-targeted therapy for NSCLC. More recently, HER2-targeted therapies have been also considered to treat NSCLC patients that harbour an HER2 mutation, mainly represented by exon 20 insertion. However, this mutation occurs in rare cases (11-14).

Taking all those observations in consideration, we aimed to refine the target population for anti-HER2 therapies in NSCLC. Keeping in mind that HER2 IHC as a single parameter was an insufficient predictive biomarker, we hypothesized that the activated HER2 form (phospho-HER2; pHER2) would be a good candidate as a relevant biomarker in NSCLC. We thus evaluated pHER2 expression in various tumours but also described molecular pathway leading to an activation of HER2, especially through the Fragile Histidine Triad (FHIT) protein. The *FHIT* gene encodes a protein with diadenosine triphosphate (Ap3A) hydrolase activity (15). FHIT loss is observed in several types of cancer especially in NSCLC and associated with a poor prognosis (16, 17). FHIT has been first described as a tumour suppressor. It reduces cell growth through several mechanisms such as the stabilisation of p53 or the repression of cyclin D1 transcription. It induces apoptosis through both the caspase 8-dependent death receptor pathway and the caspase 9-dependent mitochondrial pathway (15, 17-20). More recently, we and others have also assigned a protective role against tumour invasion and metastasis to FHIT through its ability to suppress epithelial-mesenchymal transition (EMT) in lung cancer cells. The regulation of EMT-associated genes such as E-cadherin, vimentin, fibronectin or matrix metalloproteinases by FHIT involves Src, Slug, miR-30c and/or β-catenin (19, 21-24).

Here, we investigated the relationships between FHIT and pHER2 in lung tumour cells and its clinical relevance in NSCLC. FHIT expression and HER2 activation were analysed by immunohistochemistry and western blotting in NSCLC samples and in lung tumour cell lines. Strategies of modulation of FHIT expression in lung cell lines and primary tumour cell cultures were used to study the sensitivity of tumour cells expressing or not FHIT to anti-HER2 therapy in *in vitro* and *in vivo* models of cell invasion and growth.

Materials and methods

Human tumour samples

The paraffin-embedded tumour pieces for immunohistochemistry were obtained from a cohort of 45 patients with NSCLC (Supplementary Table S1). The frozen tumour pieces used for western blot analyses were obtained from a cohort of 48 patients with NSCLC (Supplementary Table S2). Primary tumour cells were obtained from 22 NSCLC fresh samples (Supplementary Table S3).

Cell lines

Human lung cell lines HBE4-E6/E7, NCI-H2228, NCI-H441, A549, NCI-H1993, NCI-H1299, Calu-1 and SK-LU-1 were obtained from the American Type Culture Collection (Rockville, MD, USA), HCC78 from the German Collection of Microorganisms and Cell Cultures DSMZ (Braunschweig, Germany) and were cultured as described in Supplementary materials and methods.

Primary tumour cells

Freshly resected tumours were cut in small pieces, then digested overnight at +4°C in a 0.1% Pronase E solution (Sigma-Aldrich, Saint-Louis, MO) and seeded in type IV collagen coated dishes with CnT-17 medium (CELLnTEc, Bern, Switzerland). After the proliferation phase, cells were cultured in bronchial epithelial cell growth medium (BEGM) (Lonza, Walkersville, MD).

Anti-HER2 drugs

The HER2 tyrosine kinase inhibitor (TKI) irbinitinib (tucatinib, ARRY-380, ONT-380) (HY-16069) and the humanized monoclonal antibody anti-HER2 trastuzumab (HY-P9907) were purchased from MedChemtronica (Sollentuna, Sweden).

Immunohistochemistry

Immunohistochemistry for FHIT, pHER2, HER2 amplification and vimentin were performed as described in Supplementary materials and methods. The extent of pHER2 staining was graded on a scale of 0–4 (0, no staining; 1, ≤ 10%; 2, 11–25%; 3, 26–50% and 4, > 50% of positive tumour cells) and the extent of FHIT staining loss on a scale of 0–4 (0, no loss; 1, ≤ 10%; 2, 11–25%; 3, 26–50% and 4, > 50% of negative tumour cells). The scoring (0, 1+, 2+ or 3+) of HER2 amplification was evaluated by a qualified pathologist.

Western blotting

Western blot analyses were done with Mini-Protean TGX 4-20% precast gels (Bio-Rad Laboratories, Hercules, CA) and the Trans-Blot Turbo Transfer system (Bio-Rad). Following steps were performed as previously described (25).

Transfection of FHIT small interfering RNA and of FHIT expression plasmid

Cells were transfected with a mix of three siRNA duplexes (20 nM) by calcium phosphate-precipitation method as previously described (25). The sequences are described in Supplementary materials and methods. The stable transfectants NCI-H1299-FHIT and NCI-H1299-pcDNA3.1 (empty plasmid) were generated as previously described (21).

Stable transfection of CRISPR/Cas9 KO FHIT plasmid

A549 cells were co-transfected with FHIT CRISPR/Cas9 KO plasmid (h) (sc-404220, Santa Cruz Biotechnology, Santa Cruz, CA) and FHIT HDR plasmid (h) (sc-404220-HDR, Santa Cruz Biotechnology) according to the manufacturer's instructions. Sequences of gRNA are described in Supplementary materials and methods. In control cells, FHIT CRISPR/Cas9 KO plasmid (h) was replaced by Control CRISPR/Cas9 plasmid (sc-418922, Santa Cruz Biotechnology). The transfected populations were subjected to a selective pressure with puromycin. Individual clones were checked for FHIT expression by western blot analysis.

Three KO FHIT clones were selected and pooled for the experiments. Three control clones were also pooled (Supplementary Figure S1).

Immunofluorescence

Cells cultured on glass coverslips were fixed with methanol for analysis of FHIT, pHER2, vimentin and E-cadherin. Immunofluorescence was performed as previously described (21).

***In vitro* invasion models**

Boyden and spheroid invasion assays were performed as described in Supplementary materials and methods. For HER2 inhibition experiments, irbinitinib (10 nM) or trastuzumab (2 µg/ml) were added in the upper compartment of the inserts and on the top of gels, respectively. DMSO or non-immune IgG (Millipore, Temecula, CA) served respectively as negative controls.

MTT assay

HBE4-E6/E7 and A549 cells were treated with vehicle or HER2 inhibitor (10 nM irbinitinib or 2 µg/ml trastuzumab) for 2 or 7 days, respectively. Inhibitors and medium were refreshed every 2 days. Primary tumour cells were treated with growing dose of irbinitinib (1, 5, 10, 50 and 100 nM) for 7 days. For 7 days-experiments inhibitor and medium were refreshed every 2 days. MTT assays were performed as described in Supplementary materials and methods.

***In vivo* tumor xenograft model**

$2x10^6$ A549 KO FHIT or A549 control cells were inoculated s.c. with Matrigel (BD Biosciences, San Jose, CA) into the right flank of six-week-old female NMRI Nude mice (Charles River Laboratories France, L'Arbresle, France). Tumour growth was assessed by measuring the length and the width of tumours every 3-4 days. Tumour volumes were calculated using the formula: length × $width^2$ / 2. After 14 days post-inoculation, when median tumour volume reached 100-150 mm^3, mice were randomized into experimental groups (n = 10 / group). For irbinitinib experiment, irbinitinib was suspended in vehicle consisting of 5%

DMSO, 5% Cremophor EL (Sigma-Aldrich) and PBS. Irbinitinib or vehicle were administered daily at a dose of 100 mg / kg (*PO*) during 5 weeks. For trastuzumab experiment, trastuzumab was dissolved in PBS. Trastuzumab or vehicle were administered weekly at a dose of 20 mg / kg (*IP*) during 8 weeks. Mice were euthanized at the end of treatment defined by the limit point of tumour volume of 1500 mm^3. Percent relative tumour volume (RTV) values were calculated using initial (i) and final (f) tumour volume (V) measurement and the formula: $RTV\% = V_f / V_i \times 100$. Percent tumour growth inhibition (TGI) was calculated with the formula $TGI\% = (1 – T / C) \times 100$ where T is the median RTV of treated group and C the median RTV of control group.

Statistics

Two-tailed Spearman test and two-sided Fisher's exact test were used to analyse the association between parameters. Logistic regression was used to obtain ROC curves. *In vitro* data expressed as fold induction were analysed with a two-tailed one-sample Student's *t*-test. Other data were analysed with a two-tailed Mann Whitney test. $P < 0.05$ was considered significant. All analyses were performed using Prism version 5.0 software (GraphPad Software, La Jolla, CA) and XLSTAT version 2019.1.3 software (Addinsoft company, Paris, France).

Study approval

Human study was conducted in accordance with the ethical guideline of Declaration of Helsinki. Human tissues were obtained from the Tumour Bank of the Reims University Hospital Biological Resource Collection NO. DC-2008-374 declared at the Ministry of Health according to the French Law, for use of tissue samples for research. Surgically resected tumours were collected after obtaining informed consent from patients with NSCLC. Access to patient data for this retrospective non-interventional study was approved by the French national commission CNIL (Comité National de l'Information et des Libertés) (NO.2049775 v 0).

Animal study was carried out in accordance with EU Directive 2010/63/EU for animal experiments and approved by the French Ministry of National Education, Higher Education and Research (Authorization APAFIS♯4310-2016022916129092v2).

Results

A low FHIT expression is correlated with a high HER2 activation in lung tumour cells

To investigate the potential relationship between FHIT and HER2 activity, we first analysed by immunohistochemistry the expression of FHIT, the activation of HER2 (pHER2) and the overexpression of HER2 in a series of 45 human NSCLC samples including 22 adenocarcinomas (ADC) and 23 squamous cell carcinomas (SCC) (Figure 1A top, Supplementary Table S1). Twenty tumours (44.4%) had a low FHIT expression and 27 tumours (60%) were positive for pHER2 expression. The loss of FHIT expression was associated to a high activity state of HER2 ($r = 0.3563$; $p = 0.0163$). With a cut-off at median score of FHIT loss and pHER2, it was observed that $FHIT^{low}$ tumours expressed more frequently pHER2 (OR = 4.750; $p = 0.0307$). Indeed, 60% ($n = 12$) of $FHIT^{low}$ tumours expressed a $pHER2^{high}$ phenotype, which represent 26.7% of all tumours analysed, indicating a frequent and strong association in lung cancer (Figure 1A bottom). Interestingly, a high activity of HER2 was not related to its overexpression. Only 2 tumours (SCC) displayed an amplification of HER2 (score 3+), one with a score 0 and the other one with a score 4 of pHER2 (Supplementary Figure S2). A logistic regression analysis allowed to demonstrate that $FHIT^{low}$ tumours were more frequently associated with a poor tumour differentiation degree (OR = 1.494; $p = 0.045$). A same trend was observed with pHER2 considered separately ($p = 0.063$). Taking into account both FHIT loss and pHER2 parameters conjointly, the correlation with tumour differentiation status was even more relevant. Tumours with a $FHIT^{low}/pHER2^{high}$ pattern were 6 fold more frequently poorly differentiated (AUC = 0.786; $p = 0.002$). A second series of 48 NSCLC frozen samples (25 ADC and 23 SCC) was subjected to western blotting (Supplementary Table S2). We found that FHIT level was negatively correlated to activation rate of HER2 ($r = -0.4281$, $p = 0.0024$) (Figure 1B).

We thus aimed to explore this correlation *in vitro* in a series of 9 lung tumour cell lines. The presence of HER2 amplification and/or HER2 exon 20 mutation was analysed by CISH and DNA sequencing, respectively. No amplification, neither activating mutation of HER2 was detected in any cell line (Supplementary Figure S3 and Supplementary Table S4). Western blot analysis revealed a negative correlation between FHIT level and activation rate of HER2 in cell lines ($r = -0.8000$, $p = 0.0138$) (Figure 1C). Moreover, by comparing the invasive abilities in a modified Boyden chamber invasion assay, we showed that cell lines harbouring the lower FHIT level and the higher HER2 activation rate were the most invasive (Figure 1D).

FHIT expression modulation regulates HER2 activity

After demonstrating a link between FHIT expression and HER2 activity *in vivo* and *in vitro*, we studied whether FHIT was causally involved in the control of HER2 activity. We used transient transfection of FHIT siRNA or stable transfection of CRISPR/Cas9 KO FHIT plasmid to downregulate FHIT expression in FHIT-positive cell lines and a stable transfection of FHIT cDNA to overexpress FHIT in a FHIT-negative cell line. We showed that modulation of FHIT expression regulated HER2 activity. Indeed, FHIT silencing in HBE4-E6/E7, H441 and A549 cells and FHIT overexpression in H1299 cells induced respectively an increase and a decrease of HER2 activation (Figures 2A and 2B).

Therefore, we hypothesized that FHIT/pHER2 profile of lung tumour cells may determine their sensitivity to an anti-HER2 treatment. We chose to test the efficacy of two HER2 inhibitors, the TKI inhibitor irbinitinib and the humanized antibody trastuzumab. First, we analysed their effect on the phenotype of A549 KO FHIT transfectants and their control. We focused on MAPK/ERK, a pathway known to be activated by FHIT loss (24) and to be initiated downstream the phosphorylation of the tyrosine kinase domain of HER2. We observed that the concomitant activation of HER2 (pHER2) and ERK (pERK) induced by FHIT knock out was inhibited by both irbinitinib (10 nM) and trastuzumab (2 µg/ml). In addition, both inhibitors

were able to restore a more epithelial phenotype of A549 KO FHIT cells with a decrease of vimentin expression and an increase of E-cadherin localization at the cell membrane. Anti-HER2 drugs did not affect control cells (Figures 2C and 2D). These data highlighting the link between FHIT and HER2 suggested that the two drugs might affect several processes regulated by FHIT.

HER2 inhibitors reduce in vitro cell invasion and proliferation of FHIT^{low}/pHER2^{high} tumour cells

Since we previously demonstrated that FHIT was involved in the control of tumour invasion process, we explored the effect of HER2 inhibition on FHIT-dependent cell invasion *in vitro* in 2 complementary models, the modified Boyden chamber invasion assay mimicking basement membrane crossing and a 3D model of spheroids in collagen I gel mimicking cell dispersion in stroma.

In the Boyden assay, we found that FHIT siRNA-induced cell invasion was HER2-dependent. Indeed, the invasive capacities of FHIT-silenced HBE4-E6/E7 cells were decreased by 36% in the presence of irbinitinib (10 nM) and by 29% in the presence of trastuzumab (2 µg/ml) ($p = 0.002$ and 0.005, respectively) (Figures 3A top and 3B top). Irbinitinib and trastuzumab were also effective to decrease cell invasion in FHIT-silenced A549 cells (by 23%, $p = 0.028$ and by 33%, $p = 0.002$, respectively) (Figures 3A bottom and 3B bottom).

In the 3D model of spheroids, we used the stable A549 KO FHIT transfectants. In this model, we observed that FHIT silencing induced an increase of cell dispersion from the spheroids in the stroma and that this increase was counteracted by both irbinitinib (10 nM) and trastuzumab (2 µg/ml) (-21.62%, $n = 3$, $p = 0.001$ and -16.03%, $n = 4$, $p = 0.011$, respectively) (Figures 3C and 3D).

Since FHIT is known as a tumour suppressor, we also investigated the consequence of HER2 inhibition on *in vitro* tumour cell growth controlled by FHIT.

Cell proliferation analysis by MTT assay after a treatment with irbinitinib (10 nM) or trastuzumab (2 µg/ml) was done on HBE4-E6/E7 cells transiently transfected by FHIT siRNA and stable KO FHIT A549 transfectants and their respective controls. We observed that irbinitinib and trastuzumab were able to prevent specifically cell proliferation of FHIT-silenced cells whereas they had no significant effect on control cells. The increase of cell proliferation induced by FHIT silencing was reduced respectively by 29.79% and 38.64% in presence of irbinitinib ($p = 0.00045$ and $p = 0.045$) (Figure 4A) and respectively by 27.73% and 28.16% in presence of trastuzumab ($p = 0.002$ and $p = 0.002$) (Figure 4B) for HBE4-E6/E7 and A549 cells.

HER2 inhibitors reduce in vivo cell growth of $FHIT^{low}$/$pHER2^{high}$ tumour cells

In addition, we used the model of xenograft of A549 CRISPR/Cas9 KO FHIT transfectants in *nude* mice to evaluate the efficiency of an anti-HER2 treatment on tumour cell growth *in vivo* (Supplementary Figure S4). We observed that a daily oral treatment with 100 mg/kg irbinitinib inhibited the volume of KO FHIT tumours ($p = 0.0288$) whereas it had no significant effect on control tumours (Figure 5A, top left and top right). The median TGI by irbinitinib was 55.33% for KO FHIT tumours ($p = 0.0433$) (Figure 5A, bottom left). As shown by immunohistochemistry, the irbinitinib treatment resulted in a decrease of HER2 activation in KO FHIT tumour xenografts (Figure 5A, bottom right). In a second experiment, a weekly intraperitoneal administration of 20 mg/kg trastuzumab was also efficient to reduce volume of KO FHIT tumours ($p = 0.0006$) without significantly affecting control tumours (Figure B, top left and top right). The median TGI by trastuzumab was 79.98% for KO FHIT tumours ($p = 0.0006$) (Figure 5B, bottom left). In addition, KO FHIT tumours treated with trastuzumab displayed a lower pHER2 immunostaining (Figure 5B, bottom right).

FHIT^{low}/pHER2^{high} primary tumour cells from NSCLC patients are more sensitive to an anti-HER2 therapy

Finally, we decided to explore the phenotype of primary tumour cells from NSCLC patients in relation to their sensitivity to an anti-HER2 therapy. Primary tumour cells were concomitantly subjected to western blot analysis and to a treatment with growing doses of irbinitinib followed by a MTT assay. Cell sensitivity to the drug was assessed through IC50. In a global analysis, we observed again in this cohort that FHIT level was negatively correlated to activation rate of HER2 ($r = -0.5257$, $p = 0.012$) (Figure 6A). Median IC50 was 200 nM with first and third quartiles respectively at 71 and 262 nM. To find a phenotype able to predict TKI sensitivity, we performed retrospective association's tests with a cut-off at median IC50, especially on FHIT and pHER2 parameters. Fifteen tumours (68.2%) were associated with a FHIT ratio under 0.65. Twelve tumours (54.5%) expressed a pHER2 ratio higher than 0.9. Considering FHIT ratio alone, a FHIT ratio < 0.65 was associated with more sensitive tumours (OR = 12.0; $p = 0.022$), with 90.9% tumours (n = 10) harbouring a FHIT^{low} phenotype among sensitive ones. Considering pHER2 ratio independently, HER2 activation (ratio > 0.9) was also associated with tumours sensitive to irbinitinib (OR = 12.0; $p = 0.03$) with 81.8% tumours (n = 9) harbouring a high HER2 activation rate among sensitive tumours. Taking into account FHIT and pHER2 ratios conjointly, these two parameters were able to predict irbinitinib sensitivity (AUC = 0.777) (Figure 6B, top left). Indeed, a FHIT^{low}/pHER2^{high} phenotype was 45 times more often associated with an irbinitinib sensitive profile ($p = 0.0019$) (Figure 6B, top right). FHIT^{low}/pHER2^{high} primary tumour cells respond better to irbinitinib than other types of tumour cells (Figure 6B, bottom left) with a median IC50 = 77 nM versus 243 nM, respectively ($p = 0.0192$) (Figure 6B, bottom right). Interestingly, the FHIT^{low}/pHER2^{high} phenotype was significantly associated with a vimentin expression by tumour cells (OR = 8.0; $p = 0.0427$) (Supplementary Table S5).

Discussion

This study demonstrated that FHIT regulates the activity of HER2 receptor in lung tumour cells and that anti-HER2 drugs are effective to decrease the aggressiveness of FHIT-inactivated tumour cells.

First, we observed that a low FHIT expression was correlated to a high activity of HER2 *in vivo* in two series of human NSCLC cases including both adenocarcinomas and squamous cell carcinomas and *in vitro* in a panel of lung tumour cell lines. Interestingly, a high HER2 activation rate was not related to HER2 overexpression/amplification or mutation. Moreover, we showed that the modulation of FHIT expression impacts the level of activity of HER2. To our knowledge, the interplay between FHIT and HER2 pathways has been poorly described and only referred to HER2+ mammary tumours. Indeed, Bianchi *et al.* revealed that the presence of FHIT decreases the incidence of HER2-driven breast tumours in a murine model (26). The mechanism by which FHIT regulates HER2 activation remains unknown. In our context, it probably occurs through heterodimerisation with a ligand-activated HER family member. However, a direct interaction between FHIT and HER2 or its heterodimerisation partner is unlikely. The tyrosine-protein kinase Src may be a mediator of this signalling (27, 28). All these data highlight that a substantial proportion of lung tumours can display a high HER2 activity without any genetic alteration of HER2. Detection of FHIT and phospho-HER2 in NSCLC tumours could therefore bring new predictive information.

We also showed that tumours with a high activation rate of HER2, as a consequence of FHIT loss, respond to anti-HER2 drugs. Until yet, targeted therapy has been proposed to treat tumours harbouring genetic abnormalities of driver genes. The targets of such a therapy in NSCLC include EGFR mutation, MET amplification and ALK, ROS1, and RET rearrangement (29). On the other hand, we showed that the $FHIT^{low}$/$pHER2^{high}$ phenotype is associated with

dedifferentiation and features of EMT and that HER2 drugs are able to reverse, at least partially, EMT. These results are in agreement with previous studies demonstrating that loss of FHIT expression induces EMT (21-24). The presence of EMT markers is associated with poor prognoses in many carcinoma types. For instance, vimentin expression predicts the occurrence of metastases in NSCLC (30, 31). Moreover, the EMT program contributes critically to the development of resistance to conventional chemotherapy, radiotherapy as well as targeted therapy (30). In particular, activation of EMT confers resistance to EGFR-targeted therapies in NSCLC (32-34). Therefore, our data suggest that FHIT-dependent tumour cell phenotypic plasticity -which results in HER2 activation- may represent a therapeutic advantage for NSCLC. This is in agreement with the study of Tam *et al.* showing that breast carcinoma cells with an active EMT program are more vulnerable to inhibitors targeting PKCα and that of Pitts *et al.* demonstrating an association between sensitivity of colorectal cancer cells to a P21-activated kinase inhibitor and a mesenchymal molecular profile (35, 36).

A limitation of this study is the small size of cohorts. In order to validate the clinical relevance of our findings in NSCLC, as a fisrt step, FHIT/pHER2 profiling should be performed by immunohistochemistry in a larger cohort to explore its potential association with histological sub-type, stage, gender, age or smoking history. Currently, metastatic NSCLC are first evaluated on their driver oncological status (37). EGFR activating mutation, the most common and powerful actionable alteration, would probably expose to resistance to anti-HER2 therapies (38). A clinical trial could be therefore designed in a cohort with non-actionable alteration to confirm anti-HER2 efficacy and define FHIT and pHER2 levels associated with response. On another hand, a major part of patients is treated with immunotherapies such as anti-PD1 or PD-L1. However, all biomarkers failed to predict immune response even in highest PD-L1 expressors (39, 40). Because FHIT loss induces EMT which has been associated with immunotherapy resistance and poor outcomes (41, 42), it could also be interesting to confront FHIT/pHER2 and PD-L1 phenotypes to immunotherapy response in NSCLC.

In conclusion, we demonstrated that the phenotype of lung tumour cells influences the response to an HER2-targeted therapy. This study opens up new therapeutic perspectives for lung cancer in a new subclass of patients with NSCLC, including adenocarcinomas and squamous cell carcinomas harbouring a $FHIT^{low}$/$pHER2^{high}$ phenotype, which may be eligible for an anti-HER2 therapy.

Acknowledgements

This works was supported by grants from La Ligue Contre le Cancer (Committees of Marne, Haute-Marne and Moselle) and Lions Club of Soissons, Villers-Cotterets and Crépy-en-Valois. JDS was supported by the University of Reims Champagne-Ardenne. AmJ was supported by the Région Champagne-Ardenne. The authors thank Arnaud Bonnomet from PICT (Plateforme en Imagerie Cellulaire et Tissulaire, University of Reims Champagne-Ardenne) and Eymeric Lagonotte and Alexandre Abreder from INSERM UMR-S 1250 for their excellent technical assistance.

Author contributions statement

BNR and MP designed the study. JDS, AmJ, JR and BNR performed the experiments. JC and AnJ developed the plugin. JDS, AmJ, JA, VD, MD, PB, GaD, MP and BNR analysed data. GoD provided tumour samples. All authors were involved in writing the manuscript and had final approval of the submitted version.

References

1. Youlden DR, Cramb SM, Baade PD. The International Epidemiology of Lung Cancer: geographical distribution and secular trends. *J Thorac Oncol* 2008; **3:** 819-831.
2. Janku F, Stewart DJ, Kurzrock R. Targeted therapy in non-small-cell lung cancer- -is it becoming a reality? *Nat Rev Clin Oncol* 2010; **7:** 401-414.
3. Rimawi MF, Schiff R, Osborne CK. Targeting HER2 for the treatment of breast cancer. *Annu Rev Med* 2015; **66:** 111-128.
4. Waks AG, Winer EP. Breast cancer treatment: A rewiew. *JAMA* 2019; **321:** 288-300.
5. Meric-Bernstam F, Johnson AM, Dumbrava EEI, *et al.* Advances in HER2-Targeted Therapy: Novel Agents and Opportunities Beyond Breast and Gastric Cancer. *Clin Cancer Res* 2019; **25:** 2033-2041.
6. Gatzemeier U, Groth G, Butts C, *et al.* Randomized phase II trial of gemcitabine-cisplatin with or without trastuzumab in HER2-positive non-small-cell lung cancer. *Ann Oncol* 2004; **15:** 19-27.
7. Nakamura H, Kawasaki N, Taguchi M, *et al.* Association of HER-2 overexpression with prognosis in nonsmall cell lung carcinoma: a metaanalysis. *Cancer* 2005; **103:** 1865-1873.
8. Takenaka M, Hanagiri T, Shinohara S, *et al. et al.* The prognostic significance of HER2 overexpression in non-small cell lung cancer. *Anticancer Res* 2011; **31:** -4636.
9. Zinner RG, Glisson BS, Fossella FV, *et al.* Trastuzumab in combination with cisplatin and gemcitabine in patients with Her2-overexpressing, untreated, advanced non-small cell lung cancer: report of a phase II trial and findings regarding optimal identification of patients with Her2-overexpressing disease. *Lung Cancer* 2004 44: 99-110.

10. Peters S, Stahel R, Bubendorf L, *et al.* Trastuzumab Emtansine (T-DM1) in Patients with Previously Treated HER2-Overexpressing Metastatic Non-Small Cell Lung Cancer: Efficacy, Safety, and Biomarkers. *Clin Cancer Res* 2019; **25:** 64-72.
11. Barlesi F, Mazieres J, Merlio JP, *et al.* Routine molecular profiling of patients with advanced non-small-cell lung cancer: results of a 1-year nationwide programme of the French Cooperative Thoracic Intergroup (IFCT). *Lancet* 2016; **387:** 1415-1426.
12. Li BT, Ross DS, Aisner DL, *et al.* HER2 Amplification and HER2 Mutation Are Distinct Molecular Targets in Lung Cancers. *J Thoracic Oncol* 2016; **11:** 414-419.
13. Mazières J, Barlesi F, Filleron T, *et al.* Lung cancer patients with HER2 mutations treated with chemotherapy and HER2-targeted drugs: results from the European EUHER2 cohort. *Ann Oncol* 2016; **27:** 281-286.
14. Robichaux JP, Elamin YY, Vijayan RSK, *et al.* Pan-Cancer Landscape and Analysis of ERBB2 Mutations Identifies Poziotinib as a Clinically Active Inhibitor and Enhancer of T-DM1 Activity. *Cancer Cell* 2019; **36:** 444-457.
15. Silveira Zavalhia L, Weber Medeiros A, Oliveira Silva A, *et al.* Do FHIT gene alterations play a role in human solid tumors? *Asia Pac J Clin Oncol* 2018; **14:** e214-223.
16. Sozzi G, Pastorino U, Moiraghi L, *et al.* Loss of FHIT function in lung cancer and preinvasive bronchial lesions. *Cancer Res* 1998; **58:** 5032-5037.
17. Pekarsky Y, Zanesi N, Palamarchuk A, *et al.* FHIT: from gene discovery to cancer treatment and prevention. *Lancet Oncol* 2002; **3:** 748-754.
18. Zanesi N, Fidanza V, Fong LY, *et al.* The tumor spectrum in FHIT-deficient mice. *Proc Natl Acad Sci U S A* 2001; **98:** 10250-10255.
19. Weiske J, Albring KF, Huber O. The tumor suppressor Fhit acts as a repressor of beta-catenin transcriptional activity. *Proc Natl Acad Sci U S A* 2007; **104:** 20344-20349.

20. Waters CE, Saldivar JC, Hosseini SA, *et al.* The FHIT gene product: tumor suppressor and genome "caretaker". *Cell Mol Life Sci* 2014; **71:** 4577-4587.
21. Joannes A, Bonnomet A, Bindels S, *et al.* Fhit regulates invasion of lung tumor cells. *Oncogene* 2010; **29:** 1203-1213.
22. Wu DW, Lee MC, Hsu NY, *et al.* FHIT loss confers cisplatin resistance in lung cancer via the AKT/NF-κB/Slug-mediated PUMA reduction. *Oncogene* 2015; **34:** 2505-2515.
23. Suh SS, Yoo JY, Cui R, *et al.* FHIT suppresses epithelial-mesenchymal transition (EMT) and metastasis in lung cancer through modulation of microRNAs. *PLoS Genet* 2014; **10:** e1004652.
24. Joannes A, Grelet S, Duca L, *et al.* Fhit regulates EMT targets through an EGFR/Src/ERK/Slug signaling axis in human bronchial cells. *Mol Cancer Res* 2014; **12:** 775-783.
25. Polette M, Gilles C, Nawrocki-Raby B, *et al.* Membrane-type 1 matrix metalloproteinase expression is regulated by zonula occludens-1 in human breast cancer cells. *Cancer Res* 2005; **65:** 7691-7698.
26. Bianchi F, Tagliabue E, Ménard S, *et al.* Fhit expression protects against HER2-driven breast tumor development: unraveling the molecular interconnections. *Cell Cycle* 2007; **6:** 643-646.
27. Bianchi F, Magnifico A, Olgiati C, *et al*. FHIT-proteasome degradation caused by mitogenic stimulation of the EGF receptor family in cancer cells. *Proc Natl Acad Sci U S A* 2006; **103:** 18981-18986.
28. Ishizawar RC, Miyake T, Parsons SJ. c-Src modulates ErbB2 and ErbB3 heterocomplex formation and function. *Oncogene* 2007; **26:** 3503-3510.
29. Chan BA, Hughes BG. Targeted therapy for non-small cell lung cancer: current standards and the promise of the future. *Transl Lung Cancer Res* 2015; **4:** 36-54.

30. Shibue T, Weinberg RA. EMT, CSCs, and drug resistance: the mechanistic link and clinical implications. *Nat Rev Clin Oncol* 2017; **14:** 611-629.
31. Dauphin M, Barbe C, Lemaire S, *et al.* Vimentin expression predicts the occurrence of metastases in non small cell lung carcinomas. *Lung Cancer* 2013; **81:** 117-122.
32. Yauch RL, Januario T, Eberhard DA, *et al.* Epithelial versus mesenchymal phenotype determines in vitro sensitivity and predicts clinical activity of erlotinib in lung cancer patients. *Clin Cancer Res* 2005; **11:** 8686-8698.
33. Zhang Z, Lee JC, Lin L, *et al.* Activation of the AXL kinase causes resistance to EGFR-targeted therapy in lung cancer. *Nat Genet* 2012; **44:** 852-860.
34. Weng CH, Chen LY, Lin YC, *et al.* Epithelial-mesenchymal transition (EMT) beyond EGFR mutations per se is a common mechanism for acquired resistance to EGFR TKI. *Oncogene* 2019; **38:** 455-468.
35. Tam WL, Lu H, Buikhuisen J, *et al.* Protein kinase C α is a central signaling node and therapeutic target for breast cancer stem cells. *Cancer Cell* 2013; **24:** 347-364.
36. Pitts TM, Kulikowski GN, Tan AC, *et al.* Association of the epithelial-to-mesenchymal transition phenotype with responsiveness to the p21-activated kinase inhibitor, PF-3758309, in colon cancer models. *Front Pharmacol* 2013; **4:** 1-13.
37. Korpanty GJ, Graham DM, Vincent MD, *et al*. Biomarkers That Currently Affect Clinical Practice in Lung Cancer: EGFR, ALK, MET, ROS-1, and KRAS. *Front Oncol* 2014; **4:** 204.
38. Seshacharyulu P, Ponnusamy MP, Haridas D, *et al*. Targeting the EGFR signaling pathway in cancer therapy. *Expert Opin Ther Targets* 2012; **16:** 15–31.
39. Gibney, GT, Weiner LM, Atkins MB. Predictive biomarkers for checkpoint inhibitor-based immunotherapy. *Lancet Oncol* 2016; **17:** e542–e551.

40. Reck M, Rodríguez-Abreu D, Robinson AG, *et al*. Pembrolizumab versus Chemotherapy for PD-L1-Positive Non-Small-Cell Lung Cancer. *N Engl J Med* 2016; **375:** 1823–1833.
41. Raimondi C, Carpino G, Nicolazzo C, *et al*. PD-L1 and epithelial-mesenchymal transition in circulating tumor cells from non-small cell lung cancer patients: A molecular shield to evade immune system? *Oncoimmunology* 2017; **6:** e1315488.
42. Ancel J, Birembaut P, Dewolf M, *et al*. Programmed Death-Ligand 1 and Vimentin: A Tandem Marker as Prognostic Factor in NSCLC. *Cancers* 2019; **11:** 1411.

Figure legends

Figure 1: FHIT loss is correlated to HER2 activation *in vivo* and *in vitro* in human lung tumour cells. A. Top, Immunohistochemistry analysis showing FHIT, pHER2 and ampliHER2 stainings on serial sections of two ADC cases and two SCC cases (scale bar = 220 µm). Bottom, Fisher' exact test showing association between FHIT loss and HER2 activation in the entire series of NSCLC (n = 45). **B.** Western blot analysis of FHIT, pHER2 and tHER2 levels in a series of 48 cases of NSCLC. Top, Composite image of tracks from several blots to show 8 representative tumours. Levels of GAPDH served as loading controls. Bottom, Spearman test showing a negative correlation between FHIT level and HER2 activation rate (pHER2/tHER2) in the entire series of NSCLC (n = 48) (r = -0.4281; p = 0.0024). Regression line with 95% confidence interval (dashed curves) are represented. **C.** Western blot analysis of FHIT, pHER2 and tHER2 levels in a series of 9 lung tumour cell lines. Top, Blots of cell lines. Levels of GAPDH served as loading controls. Middle, Quantification graphs. Bottom, Spearman test showing a negative correlation between FHIT level and HER2 activation rate (pHER2/tHER2) in the cell lines (n = 9) (r = -0.8000; p = 0.0138). Regression line with 95% confidence interval (dashed curves) are represented. **D.** Analysis of invasive capacities of the cell lines in a modified Boyden chamber assay. Values represent means ± SD. Abbreviations: pHER2, phospho-HER2; ampliHER2, amplified HER2; tHER2, total HER2.

Figure 2: Modulation of FHIT expression regulates HER2 activation. **A.** Western blot analysis of FHIT, pHER2 and tHER2 levels after FHIT silencing in HBE4-E6/E7, H441 and A549 cell lines transiently transfected by FHIT siRNA or the scrambled control, in A549 cell line stably transfected by CRISPR/Cas9 KO FHIT plasmid or the control plasmid and after FHIT overexpression in H1299 cell line stably transfected by FHIT cDNA or the control empty plasmid. GAPDH served as loading control. **B.** Immunofluorescence detection of FHIT and pHER2 (red) in A549 CRISPR/Cas9 KO FHIT transfectants and their control. Nuclei were

counterstained with DAPI (blue). (scale bar = 34 µm). **C**. Western blot analysis of FHIT, pHER2, tHER2, pERK, tERK, vimentin and E-cadherin levels in A549 CRISPR/Cas9 KO FHIT transfectants and their control treated or not with irbinitinib (10 nM) (top) or trastuzumab (2 µg/ml) (bottom). Cells were treated 3 h for analysis of HER2 and ERK activation and 24 h for other proteins. GAPDH served as loading control. **D.** Immunofluorescence detection of vimentin and E-cadherin (red) in A549 CRISPR/Cas9 KO FHIT transfectants and their control treated 24 h or not with irbinitinib (10 nM) (top) or trastuzumab (2 µg/ml) (bottom). Nuclei were counterstained with DAPI (blue). (scale bar = 34 µm). Abbreviations: pHER2, phospho-HER2; tHER2, total HER2, pERK, phospho-ERK; tERK, total ERK.

Figure 3: HER2 inhibitors reduce *in vitro* cell invasion of FHIT^{low}/pHER2^{high} tumour cells. Analysis of cell invasion capacities in a matrigel modified Boyden chamber assay of FHIT siRNA-transfected HBE4-E6/E7 and A549 cell lines treated or not with irbinitinib (10 nM) (n = 3 and n = 4, respectively) **(A)** or trastuzumab (2 µg/ml) (n = 4 and n = 4, respectively) **(B)**. Values represent means ± SD. One sample t-test, * $p < 0.05$; ** $p< 0.01$. Timelapse videomicroscopy of tumor cell dispersion from spheroids of A549 CRISPR/Cas9 KO FHIT transfectants and their control into a collagen I matrix treated or not with irbinitinib (10 nM) **(C)** or trastuzumab (2 µg/ml) **(D)**. Top, Representative phase-contrast images of spheroids at T0 and T = 72h (scale bar = 48 µm). Bottom, Representative time course analysis of mean relative area of spheroids. Endpoint values were compared using Mann-Whitney test. $n \geq 8$ for each condition. ** $p< 0.01$; *** $p< 0.001$.

Figure 4: HER2 inhibitors reduce *in vitro* cell proliferation of FHIT^{low}/pHER2^{high} tumour cells. Cell proliferation analysis by MTT assay after a treatment of 2 days of FHIT siRNA-transfected HBE4-E6/E7 cells (top) and of 7 days of A549 CRISPR/Cas9 KO FHIT transfectants (bottom) and their respective controls with irbinitinib (10 nM) **(A)** or trastuzumab

(2 µg/ml) **(B)**. Values represent means ± SD (n = 3 and 4 experiments, respectively). One sample t-test, * $p < 0.05$; ** $p < 0.01$; *** $p < 0.001$.

Figure 5: HER2 inhibitors reduce *in vivo* tumour cell growth of FHIT^{low}/pHER2^{high} tumour cells. A. Top left, Comparison by Mann-Whitney test of individual tumour volumes at endpoint of treatment with irbinitinib (100 mg/kg/d) of mice grafted with A549 CRISPR/Cas9 KO FHIT transfectants or their control (bars = median). Top right, Photographs of representative tumours of each group of mice at endpoint of irbinitinib treatment. Bottom left, Tumour growth curves of A549 CRISPR/Cas9 KO FHIT and control xenografts as a function of time of treatment with irbinitinib. Values represent median relative volume (RTV) and interquartile range (IQR). Endpoint RTV were compared using Mann-Whitney test. n = 10. Bottom right, Immunohistochemistry analysis showing pHER2 staining on sections of representative tumour xenografts (scale bar = 110 µm). **B.** Top left, Comparison by Mann-Whitney test of individual tumour volumes at endpoint of treatment with trastuzumab (20 mg/kg/w) of mice grafted with A549 CRISPR/Cas9 KO FHIT transfectants or their control (bars = median). Top right, Photographs of representative tumours of each group of mice at endpoint of trastuzumab treatment. Bottom left, Tumour growth curves of A549 CRISPR/Cas9 KO FHIT and control xenografts as a function of time of treatment with trastuzumab. Values represent median relative volume (RTV) and interquartile range (IQR). Endpoint RTV were compared using Mann-Whitney test. n = 10 except KO FHIT+ vehicle group n = 9. Bottom right, Immunohistochemistry analysis showing pHER2 staining on sections of representative tumour xenografts (scale bar = 110 µm). ** $p< 0.01$; *** $p< 0.001$; NS: non significant. Abbreviations: pHER2, phospho-HER2.

Figure 6: NSCLC cells with a FHIT^{low}/pHER2^{high} phenotype are more sensitive to an anti-HER2 therapy. A. Western blot analysis of FHIT, pHER2 and tHER2 levels in a series of NSCLC primary cultures. Left, Blots of 8 representative primary tumour cultures are shown.

Levels of GAPDH served as loading controls. Right, Spearman test showing a negative correlation between FHIT level and HER2 activation rate (pHER2/tHER2) in the entire series of 22 primary cell cultures (r = -0.5257; p = 0.0120). Regression line with 95% confidence interval (dashed curves) are represented. Vertical and horizontal grey lines represent respectively the cut-off of FHIT level (0.65) and of pHER2/tHER2 ratio (0.9) determined by retrospective association's tests. Grey dots represent tumour cells with a $FHIT^{low}/pHER2^{high}$ profile (n = 10) and black dots represent other types of tumour cells (comprising $FHIT^{high}/pHER2^{low}$, n = 5; $FHIT^{high}/pHER2^{high}$, n = 2; and $FHIT^{low}/pHER2^{low}$, n = 5). **B.** Analysis by MTT assay of response of primary tumour cells to growing doses of irbinitinib. Top left, ROC curve showing the specificity of FHIT and pHER2 parameters to predict sensitivity to irbinitinib (AUC = 0.777). Top right, Fisher' exact test showing association between $FHIT^{low}/pHER2^{high}$ phenotype and irbinitinib sensitivity. Bottom left, Log-dose response curves to irbinitinib. Values represent median and interquartile range. Bottom right, IC50 were compared using Mann-Whitney test (bars = median). * $p < 0.05$. Abbreviations: pHER2, phospho-HER2.

Supplementary Information Online

Supplementary materials and methods.

Figure S1. Analysis of FHIT expression level of A549 CRISPR/Cas9 clones.

Figure S2. HER2 activation is not correlated to HER2 overexpression/amplification in NSCLC.

Figure S3. Analysis of HER2 status of lung tumor cell lines.

Figure S4. Characterization of A549 CRISPR/Cas9 transfectants used in *in vivo* tumor xenograft model.

Table S1. Description of the population studied by immunohistochemistry.

Table S2. Description of the population studied by western blotting.

Table S3. Description of the population studied by MTT assay.

Table S4. Results of HER2 mutation and amplification screening in lung tumor cell lines.

Table S5. Association between $FHIT^{low}$/$pHER2^{high}$ phenotype and vimentin positivity in primary tumor cells from NSCLC patients.

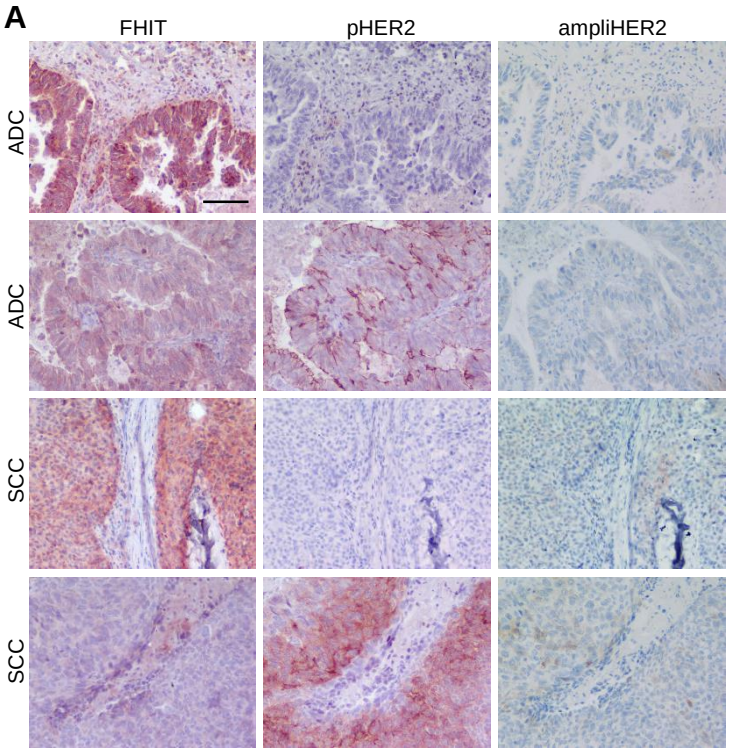

Variable	FHIT loss 0-50% (n = 25)	FHIT loss > 50% (n = 20)	OR [95% CI]	p
pHER2 0-10% (n = 27)	19 (70.4%)	8 (29.6%)	4.750 [1.318 – 17.12]	0.0307
pHER2 > 10% (n = 18)	6 (33.3%)	12 (66.7%)		

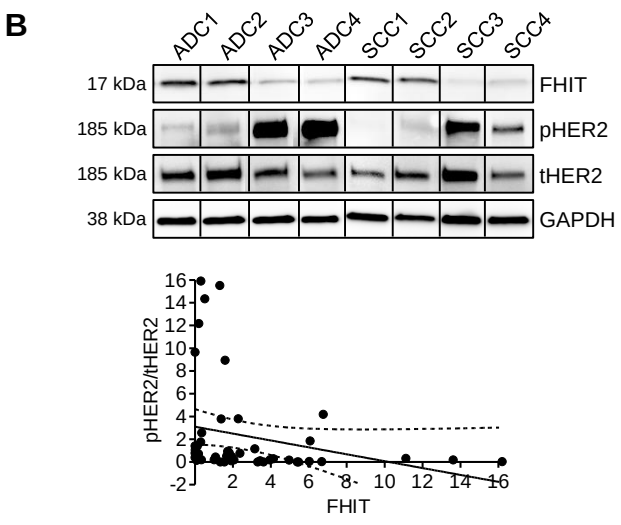

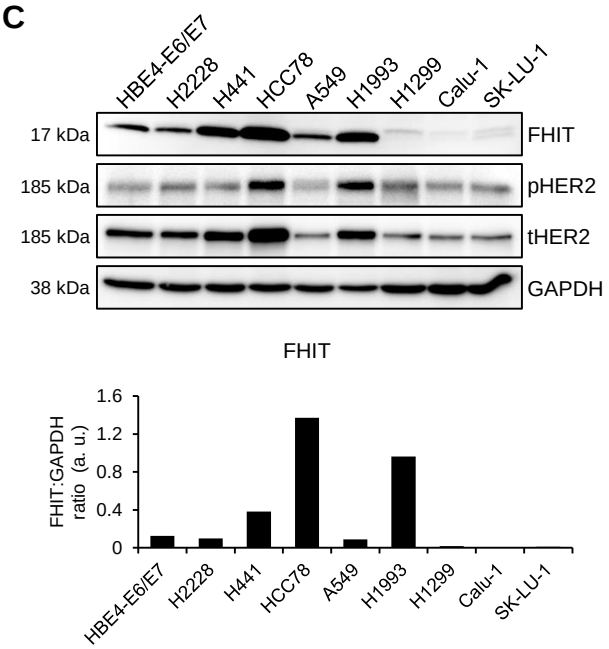

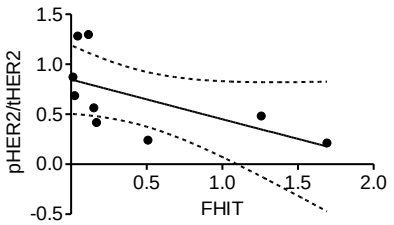

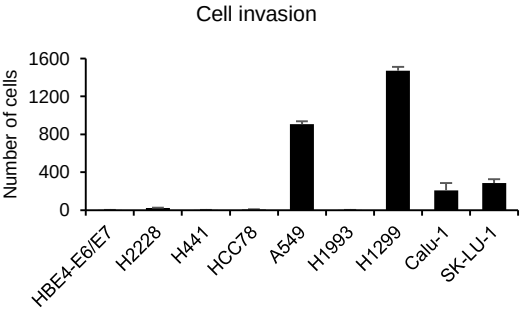

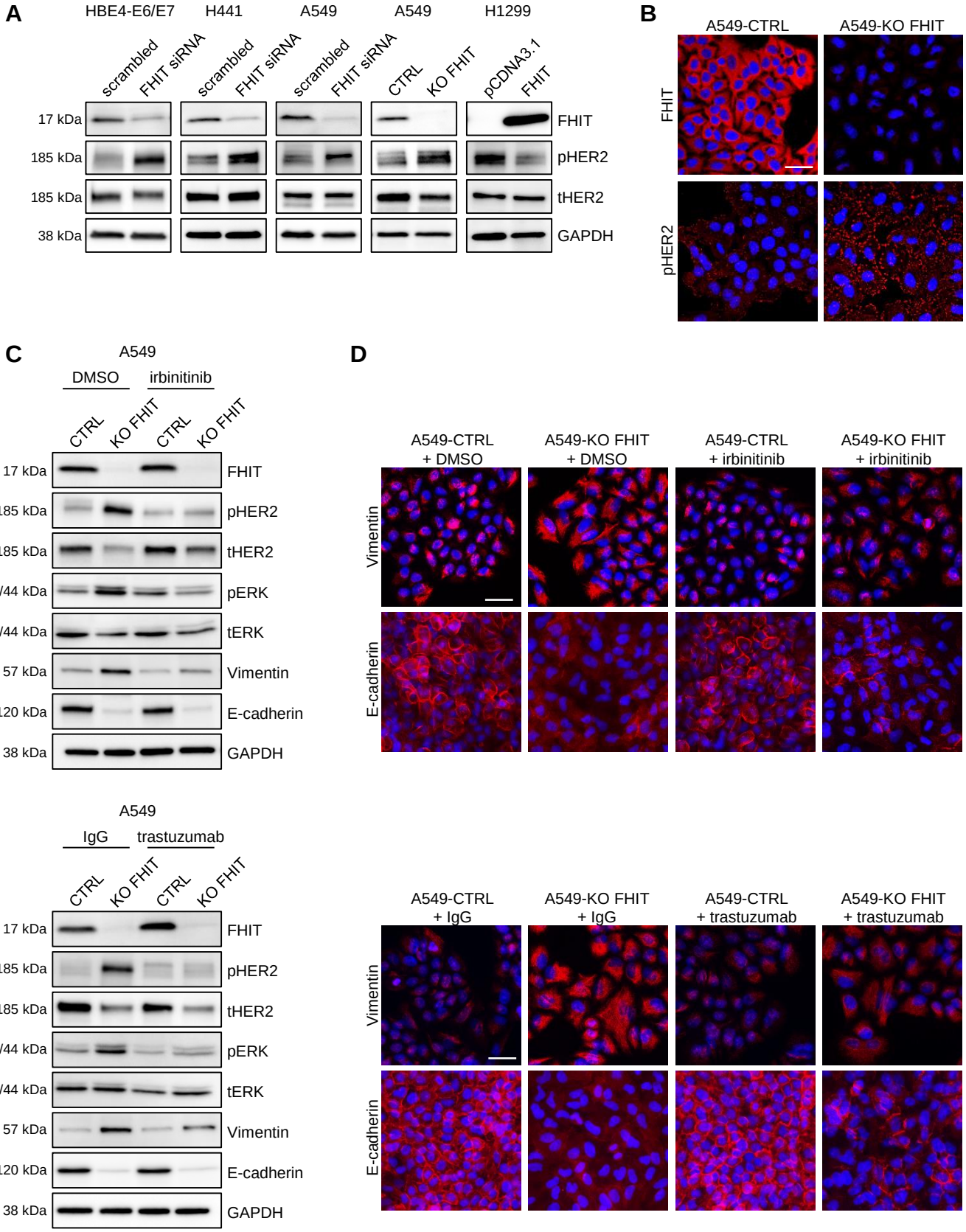
A
HBE4-E6/E7
H441
A549
A549
H1299
scrambled
FHIT siRNA
scrambled
FHIT siRNA
scrambled
FHIT siRNA
CTRL
KO FHIT
pCDNA3.1
FHIT
17 kDa
185 kDa
185 kDa
38 kDa
FHIT
pHER2
tHER2
GAPDH
B
A549-CTRL
A549-KO FHIT
FHIT
pHER2
C
A549
DMSO
irbinitinib
CTRL
KO FHIT
CTRL
KO FHIT
17 kDa
185 kDa
185 kDa
42/44 kDa
42/44 kDa
57 kDa
120 kDa
38 kDa
FHIT
pHER2
tHER2
pERK
tERK
Vimentin
E-cadherin
GAPDH
A549
IgG
trastuzumab
CTRL
KO FHIT
CTRL
KO FHIT
17 kDa
185 kDa
185 kDa
42/44 kDa
42/44 kDa
57 kDa
120 kDa
38 kDa
FHIT
pHER2
tHER2
pERK
tERK
Vimentin
E-cadherin
GAPDH
D
A549-CTRL
+ DMSO
A549-KO FHIT
+ DMSO
A549-CTRL
+ irbinitinib
A549-KO FHIT
+ irbinitinib
Vimentin
E-cadherin
A549-CTRL
+ IgG
A549-KO FHIT
+ IgG
A549-CTRL
+ trastuzumab
A549-KO FHIT
+ trastuzumab
Vimentin
E-cadherin

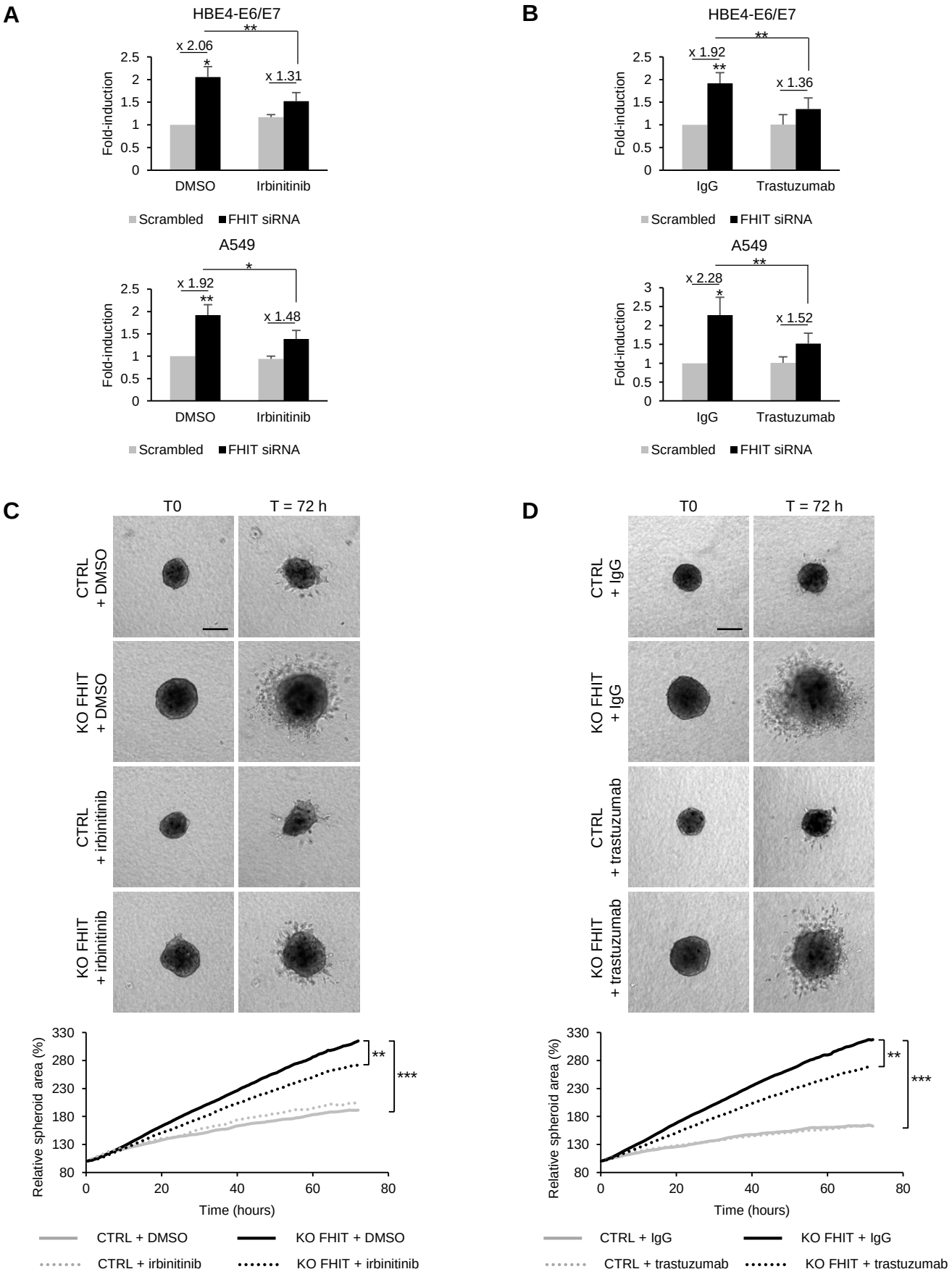
A
HBE4-E6/E7
x 2.06
x 1.31
Fold-induction
DMSO
Irbinitinib
Scrambled
FHIT siRNA
A549
x 1.92
x 1.48
B
HBE4-E6/E7
x 1.92
x 1.36
IgG
Trastuzumab
A549
x 2.28
x 1.52
C
T0
T = 72 h
CTRL + DMSO
KO FHIT + DMSO
CTRL + irbinitinib
KO FHIT + irbinitinib
Relative spheroid area (%)
Time (hours)
CTRL + DMSO
KO FHIT + DMSO
CTRL + irbinitinib
KO FHIT + irbinitinib
D
CTRL + IgG
KO FHIT + IgG
CTRL + trastuzumab
KO FHIT + trastuzumab

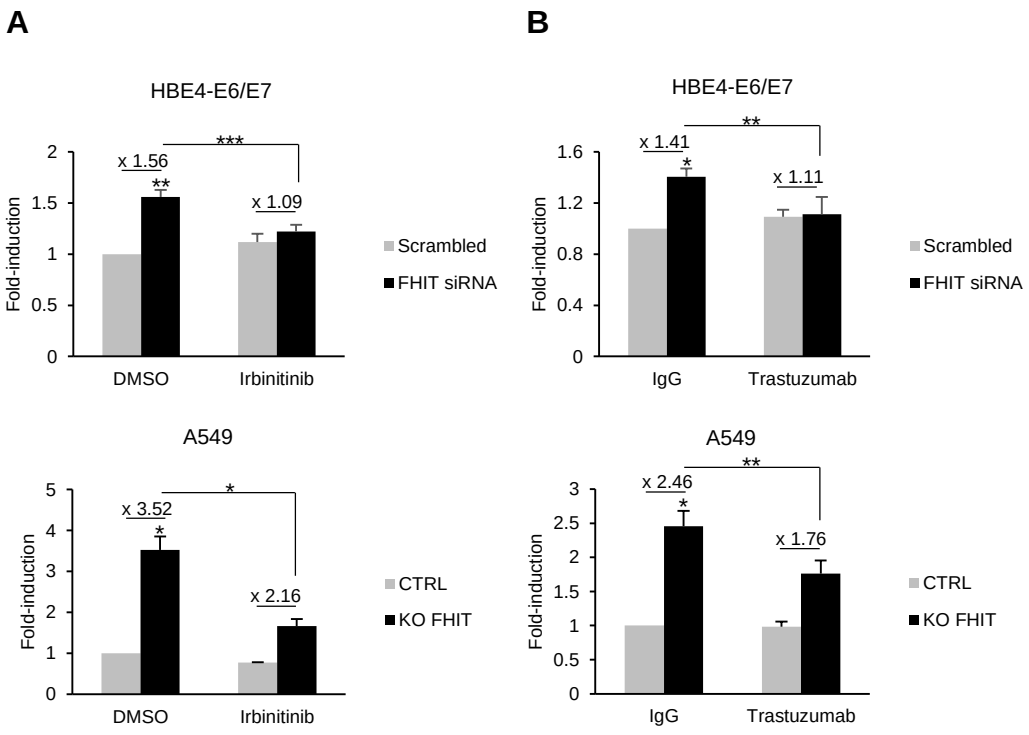
A
HBE4-E6/E7
Fold-induction
x 1.56
***
**
x 1.09
DMSO
Irbinitinib
Scrambled
FHIT siRNA
A549
x 3.52
*
x 2.16
CTRL
KO FHIT
B
HBE4-E6/E7
x 1.41
**
*
x 1.11
IgG
Trastuzumab
A549
x 2.46
x 1.76

A

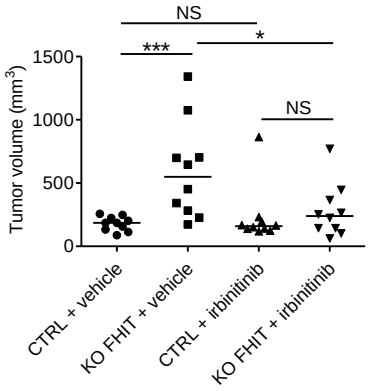
NS
***
*
NS
Tumor volume (mm3)
1500
1000
500
0
CTRL + vehicle
KO FHIT + vehicle
CTRL + irbinitinib
KO FHIT + irbinitinib

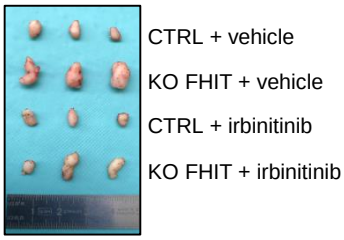
CTRL + vehicle
KO FHIT + vehicle
CTRL + irbinitinib
KO FHIT + irbinitinib

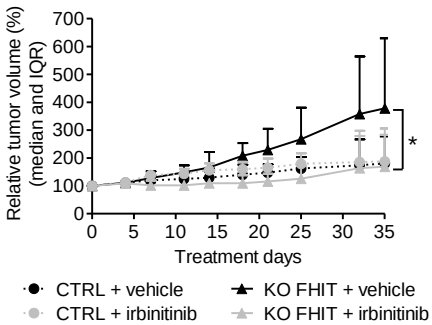
Relative tumor volume (%)
(median and IQR)
700
600
500
400
300
200
100
0
0 5 10 15 20 25 30 35
Treatment days
*
CTRL + vehicle
KO FHIT + vehicle
CTRL + irbinitinib
KO FHIT + irbinitinib

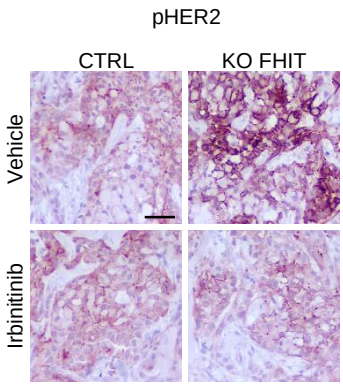
pHER2
CTRL
KO FHIT
Vehicle
Irbinitinib

B

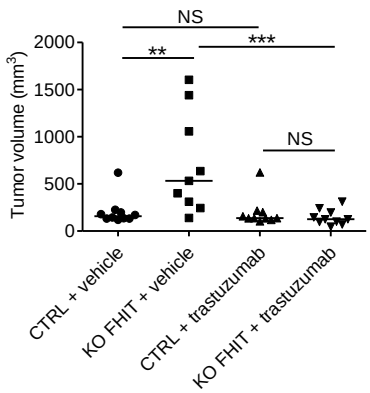
NS
**
***
NS
Tumor volume (mm3)
2000
1500
1000
500
0
CTRL + vehicle
KO FHIT + vehicle
CTRL + trastuzumab
KO FHIT + trastuzumab

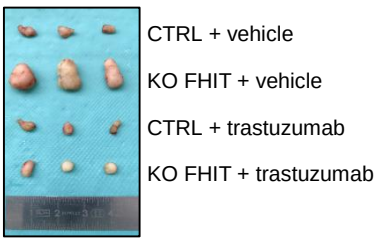
CTRL + vehicle
KO FHIT + vehicle
CTRL + trastuzumab
KO FHIT + trastuzumab

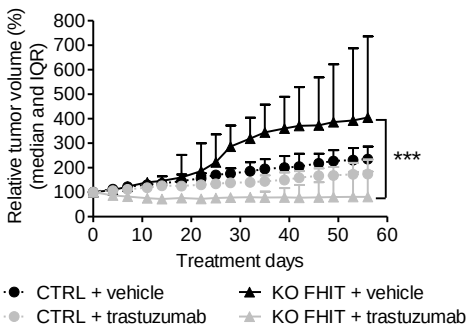
Relative tumor volume (%)
(median and IQR)
800
700
600
500
400
300
200
100
0
0 10 20 30 40 50 60
Treatment days
***
CTRL + vehicle
KO FHIT + vehicle
CTRL + trastuzumab
KO FHIT + trastuzumab

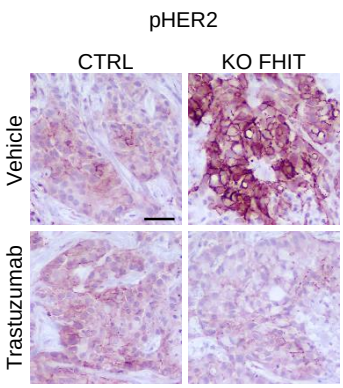
pHER2
CTRL
KO FHIT
Vehicle
Trastuzumab

A

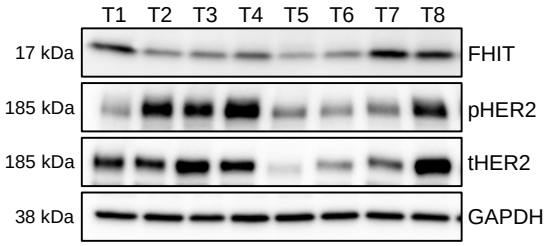

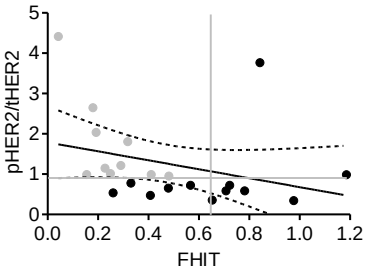

B

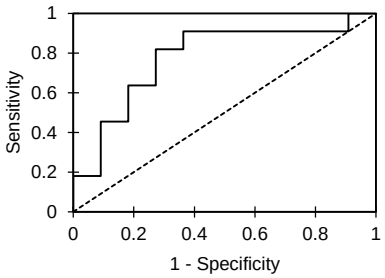

Variable	FHIT^{low}/pHER2^{high} (n = 10)	Others (n = 12)	OR [95% CI]	p
IC50 < 200 nM (n = 11)	9 (81.8%)	2 (18.2%)	45.000 [3.463 – 584.7]	0.0019
IC50 > 200 nM (n = 11)	1 (9.1%)	10 (90.9%)